Raman Spectroscopy for Spinline Crystallinity Measurements. I. Experimental Studies

Rajesh P. Paradkar, Rajen M. Patel, Ed Knickerbocker, Antonios Doufas*

Dow Chemical Company, 2301 North Brazosport Boulevard, Freeport, Texas 77541

Received 6 December 2007; accepted 18 March 2008
DOI 10.1002/app.28388
Published online 27 May 2008 in Wiley InterScience (www.interscience.wiley.com).

ABSTRACT: Online Raman spectra, obtained at different points along the spinline during the melt spinning of polypropylene homopolymer (hPP) fibers, are presented. The percentage crystallinity corresponding to each spectrum was determined from the normalized intensity of the 809-cm^{-1} Raman band. A calibration curve for propylene crystallinity was established offline with compression-molded films and fibers spun under different processing conditions. Several hPPs and propylene–ethylene copolymers (with 5–15% ethylene) were used to cover a wide calibration range for propylene crystallinity (9.5–60.9%) with an R^2 value of 0.989. This calibration curve was subsequently used to predict the polypropylene crystallinity in the spinline as a function of distance from the spinneret. Under identical conditions of quench and throughput, at a fixed point along the spinline, the overall crystallinity developed in the fiber was found to increase with an increase in the spinning speed. As the spinning speed increased, the point of the onset of crystallization moved closer to the spinneret. The rise in crystallinity was more gradual, at 750 m/min as opposed to 1500 m/min. Increasing the throughput at constant spinning speed was found to decrease the rate of crystallization because of a decrease in the spinline stress. At a fixed distance from the spinneret under identical conditions of quench and spinning speed, fibers spun at a higher throughput showed less overall crystallinity. The onset and rate of crystallization was found to be faster in the lower melt index H502-25RG resin as compared to the 5D49 resin under the spinning conditions explored. The experimental data presented here were used to validate fundamental fiber-spinning models (see part II of this series of articles). The validated models and experimental observations can be used to guide the fiber spinning of isotactic polypropylene for rapid product development. J Appl Polym Sci 109: 3413–3420, 2008

Key words: crystallization; fibers; poly(propylene) (PP); Raman spectroscopy

INTRODUCTION

A number of well-known methods are available for the determination of crystallinity in semicrystalline polymers. Crystallinity is commonly derived from heat of fusion, density, X-ray diffraction (XRD), and NMR measurements. However, most of these methods are not amenable for on spinline crystallinity measurements. In an attempt to understand how fiber crystallinity develops in the spinline, online X-ray patterns, as a function of distance from the spinneret, have been obtained during actual fiber spinning.[1] However, most of this work has traditionally been accomplished with high-intensity synchrotron X-ray radiation.[2–5] A vibrational spectroscopic technique such as Raman spectroscopy offers several distinct advantages for *in situ* crystallinity measurements in the spinline. Raman spectroscopy does not require an elaborate experimental setup like XRD and can also provide detailed morphological information on both the amorphous and crystalline phases of the polymer, provided that the vibrational bands characteristic of each phase can be unambiguously identified. Raman spectroscopy typically involves the use of visible or near-infrared radiation, which is very amenable to fiber-optic coupling with standard low-cost silica fibers (several hundred meters in ideal cases). In addition, because Raman spectroscopy is a scattering phenomenon, it also requires no sample preparation. Polymer powders, pellets, molded articles, fibers (circular and noncircular cross sections), and films can be probed by simply illumination with a laser beam and analysis of the backscattered radiation. Raman spectroscopy has been used to monitor crystallinity development in polyethylene fibers[6] and blown films[7] and relative orientation in polypropylene (PP) fibers.[8]

In this article, the first of a two-part series, we report the online crystallinity data for polypropylene homopolymer (hPP) fibers acquired to develop and validate fundamental fiber-spinning models. An evaluation of available Raman vibrations for crystallinity measurement in PP is also presented. The results from the validation and refinement of fundamental fiber-spinning models with the data presented here will be presented in the second part of this series.

Correspondence to: R. P. Paradkar (rparadkar@dow.com).
**Present address*: Sunoco, Inc., Pittsburgh, PA 15219.

TABLE I
Vibrational Assignments for the Major Raman Bands of *i*-PP

Raman band (cm^{-1})	Vibrational assignment[a]
809	$r(CH_2)$, ν(C—C)
841	$r(CH_2)$
972	$r(CH_3)$,ν(C—C)
998	$r(CH_3)$
1151	ν(C—C), δ(CH)
1167	ν(C—C), $r(CH_3)$, ω(C—C)
1218	$t(CH_2)$, ω(CH), ν(C—C)
1435	$\delta(CH_2)$
1458	$\delta(CH_2)$

[a] From refs. 10 and 11. δ = bending; *r* = rocking; ν = stretching; *t* = twisting; ω = wagging.

Semicrystalline polymers, such as PP, have a heterogeneous microstructure and consist of crystalline and noncrystalline domains. To determine the crystallinity, it is, therefore, necessary to identify the appropriate Raman bands that originate due to scatter from these three-dimensional crystalline domains. The interchain interactions within the crystals lowers the symmetry and leads to band splitting or the activation of previously forbidden vibrational bands. These are true crystallinity bands; that is, they require three-dimensional ordering for their observation. Unfortunately, true crystallinity bands are actually quite rare and are typically not observed in the vibrational spectrum at room temperature. These bands can sometimes be observed for certain polymers only when the sample is cooled to a very low temperature to improve band resolution. As a result, vibrational spectroscopic techniques (Raman and infrared) are primarily only sensitive to conformational order/disorder (regularity) along the chain length and are usually less sensitive to the three-dimensional (lateral) order of the crystalline phase. However, if an appropriate spectral marker for a given phase can be found, Raman spectra for samples with a wide range of crystallinities can be recorded and correlated with an appropriate independent measure of crystallinity, such as density, differential scanning calorimetry (DSC), or wide-angle XRD.[9]

In isotactic polypropylene (*i*-PP), the individual chains in the crystals lie in 3_1 helices with each unit cell containing four chains. Two of these chains rotate upward, whereas the other two rotate down.[10] PP chains in the amorphous regions have isomeric defects and are, thus, not capable of forming regular helices required for crystallization. Because conformational regularity is a necessary prerequisite for the formation of regular helical sequences and, consequently, crystallization, the assignment of Raman bands to a specific phase may be achieved on the basis of the conformational regularity of the chains; that is, if bands arising because of highly regular helical sequences can be identified, they can be used as spectral markers for the crystalline phase. Put differently, Raman bands due to highly regular chains/helical sequences have a higher probability of being associated with the crystalline domains and, hence, can be indicative of the crystallinity. The intensity of such bands should, therefore, correlate well with the concentration of the crystals measured with an independent technique.

Because of a lack of translational symmetry in the nonhelical chains, there is no coupling between the molecular vibrations of the neighboring repeat units as their motions cancel out along the length of the polymer chain. Each repeat unit essentially behaves as an isolated molecule in its own environment, and the Raman spectrum reflects the fundamental modes of the chemical repeat units.[11,12] However, in regular helical sequences, because of translational symmetry, the fundamental vibrations of each repeat unit within a single polymer chain (intrachain) are coupled when they vibrate in phase.[9,11,12] As a result, the fundamental frequencies split into modes characteristic of the helical chain sequences. These are referred to as the *regularity modes.*[10–12] These modes can be used as spectral markers for the crystalline phase because they depend on the conformation of the individual chains that arise from sections of the chain that have a regular 3_1 helical structure.

The Raman spectrum of PP has been extensively discussed in the open literature, and key vibrational assignment are shown in Table I.[10,11,13] The Raman spectra of *i*-PP as a function of temperature are shown in Figure 1. On the basis of our earlier discussion, peaks that do not disappear upon melting are those that can be assigned to group frequencies. Peaks that disappear in the melt are those that can be assigned to the helical chain conformation or crystal unit cell.[11] These peaks disappear upon melting because the regular helices are destroyed. On

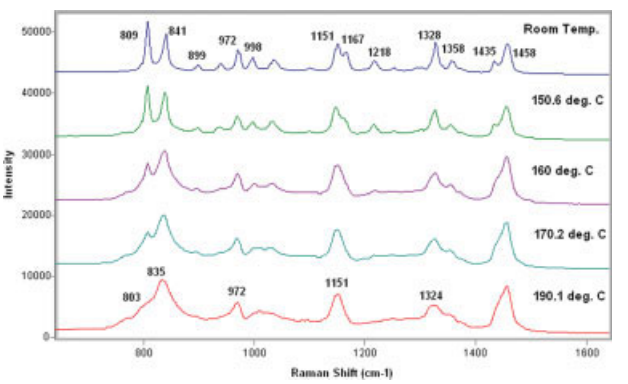

Figure 1 Raman spectra of *i*-PP as a function of temperature. [Color figure can be viewed in the online issue, which is available at www.interscience.wiley.com.]

this basis, Raman bands at 809, 841, 899, 998, 1167, and 1218 cm^{-1} must be associated with the helical structure. This is in good agreement with the calculated normal vibrational modes of *i*-PP.[10,13] The Raman peaks at 972 and 1151 cm^{-1} are present in the melt and in the partially crystalline state and must, therefore, be due to fundamental frequencies of the chemical repeat unit. The broadening of these bands in the melt is likely due to an increase in disorder. The 1151-cm^{-1} band is present in both *i*-PP and syndiotactic PP and is, therefore, unlikely to be specific to chain conformation.[14] The 972-cm^{-1} band is associated with short helical segments but also contains a component specific for chains in disordered regions having irregular conformations.[10,13] In addition, this band arises because of vibrations that are highly localized in the $—CH_3$ group,[10] and as a result, the appearance of this band is only weakly affected by neighboring repeat units. This likely explains the occurrence of this band in the melt.

Several authors have reported that in a vibrational spectrum, regularity bands only appear for certain minimum lengths of the helical sequences.[15–17] It has been reported that a minimum sequence length of five units is required for the 972-cm^{-1} band, although strictly speaking, this band also has a component specific for chains in disordered regions. The minimum sequence length for the 998-cm^{-1} band is between 5 and 10 propylene units. The band at 841 cm^{-1} requires a minimum sequence length of 12–14, whereas the bands at 809 and 1218 cm^{-1} are associated with slightly longer sequences of at least 15 propylene units.[18,19] This is in good qualitative agreement with the data shown in Figure 1. With an increase in temperature, the intensities of the 809- and 1218-cm^{-1} bands, associated with longer sequences, are considerably diminished. In fact, the 1218-cm^{-1} band is barely visible in the spectrum at about 170°C. Longer, regular helical sequences are more likely to be associated with the crystalline domains. As the temperature is increased, the number of defects in the crystalline region increases due to an increase in entropy. It is, therefore, conceivable that bands associated with longer helical sequences would significantly weaken because the conformational defects effectively disrupt the longer range intrachain correlations. On the other hand, bands associated with shorter helical sequences (e.g., the band at 998 cm^{-1}), although significantly broader, are still visible near the melting point. This suggests that some conformational order/short helical sequences still persist and may not be completely destroyed even in the melt. Interestingly, the 972-cm^{-1} band in the melt is fairly intense, which confirms that this band contains a component specific for chains in disordered regions having irregular conformations. The 809- and 1218-cm^{-1} Raman peaks, therefore, appear to be likely spectral markers for the estimation of crystallinity in *i*-PP.

A comparison of the PP spectrum at room temperature with that of the melt spectrum at 190°C indicates that the Raman band at 835 cm^{-1} splits into two bands at 809 and 841 cm^{-1} upon crystallization. Thus, the 835-cm^{-1} band most likely represents a fundamental frequency of the chemical repeat unit, whereas the 809- and 841-cm^{-1} bands likely arise because of correlation splitting. Correlation splitting due to interchain (crystal) interactions in the unit cell has been reported for the 809-cm^{-1} band below −196°C.[20] Although weak, observed correlation splitting for this band strongly suggests that this particular regularity mode is most likely related to the helical sequences within the crystals. On the other hand, the 841-cm^{-1} band is primarily assigned to the $—CH_3$ rock mode and has been shown to be associated with helical chains where the trans–gauche conformation has been disrupted.[14] In fact, intensity ratio of the 841 cm^{-1} and 809 cm^{-1} Raman bands (I_{841}/I_{809}) has been reported to increase with an increase in the kinking of the trans–gauche conformation.[21] Thus, unlike the 809-cm^{-1} band, the 841-cm^{-1} Raman band is associated with helical chains with isomeric defects.

From a practical standpoint, the 809-cm^{-1} Raman band is very intense (the most intense band in the Raman spectrum) and is also fairly well resolved, which thereby makes it ideal for spinline crystallinity measurements. In contrast, the 1218-cm^{-1} band, although better resolved, is very weak and, thus, is not very amenable for online work [lower signal-to-noise ratio (S/N)]. More importantly, however, unlike the 1218-cm^{-1} band (see Table I), the 809-cm^{-1} band is related only to the $—CH_3$ rock and —C—C— backbone stretch. In this study, the 809-cm^{-1} Raman peak was, therefore, selected as a spectral marker for the estimation of crystallinity in *i*-PP. A calibration curve was first developed offline by the correlation of the normalized intensity of the 809-cm^{-1} Raman peak with the sample crystallinity measured with DSC. This calibration curve was subsequently used to predict the crystallinity from the Raman spectra measured as a function of distance from the spinneret.

EXPERIMENTAL

Calibration samples

The calibration curve for propylene crystallinity was developed with samples consisting of fibers spun under different processing conditions and air-cooled, compression-molded plaques. A total of 23 (fiber and film) samples were prepared to develop the calibration model. The fiber and plaque samples were prepared from different *i*-PP homopolymer and pro-

pylene–ethylene copolymer (with 5–15 wt % ethylene) resins to cover a wide range of propylene crystallinity (ca. 9.5–60.9%).

Measurement of the crystallinity

The crystallinity of the calibration samples was measured with a TA Instruments (New Castle, DE) DSC Q 1000. Typically, 3–7 mg of the fiber sample was heated at 10°C/min. The heat of fusion from the first heat was used to calculate the propylene crystallinity. A value of 165 J/g was used for the heat of fusion corresponding to a perfect PP crystal (ΔH^o). The rationale for selecting this value of ΔH^o is presented next.

ΔH^o

Several different values, ranging from 148 to 210 J/g,[22] have been reported for ΔH^o of 100% crystalline PP, with an average of about 165 J/g.[23,24] Because the Raman data were calibrated with DSC, an appropriate value for ΔH^o had to be selected to ensure the accuracy of the calibration model. The ΔH^o value of 165 J/g, used in this study, was confirmed as follows. Sample plaques were compression-molded from a select set of homopolymer and copolymer resins. The plaques were aged for 2 weeks, and their crystallinity was measured by XRD and DSC. The DSC data were acquired as described earlier. XRD data were acquired with a Bruker-AXS (Madison, WI) D8 Advantage diffractometer equipped with a Cu X-ray tube source and a Vantech detector. Data were collected through a 2θ range from 4 to 60° at a rate of 0.5° 2q/min. The XRD data were analyzed with JADE XRD (MDI, Livermore, CA) (version 7.1) pattern processing software. The measured heat of fusion for the samples tested are shown in Table II along with the corresponding values of percentage crystallinity obtained via XRD. These two values were used to calculate the limiting value for ΔH^o of 100% crystalline PP. As seen, an average value of approximately 170 J/g was obtained from a comparison of the XRD and DSC data for all of the samples. A ΔH^o value of 165 J/g was, therefore, justified for the heat of fusion of 100% crystalline PP.

TABLE II
Comparision of the Percentage Crystallinity as Measured by XRD and DSC for Select Resins

Sample	Ethylene (wt %)	Measured $\%X_c$ (X-ray)	Measured ΔH (J/g)	Calculated ΔH^o (J/g)
hPP 1	0	63	105	167
hPP 2	0	58	103	178
PE copolymer 1	3	53	91	172
PE copolymer 2	5	42	73	173
PE copolymer 3	9	29	48	167
PE copolymer 4	12	18	30	164

PE copolymer = propylene–ethylene copolymer.
$\%X_c$, percent crystallinity; ΔH, heat of fusion (J/g).

Raman data collection

Raman spectra were acquired on a Kaiser Optical Systems Holoprobe Raman spectrometer (Ann Arborn, MI) equipped with a remote fiber optic probe. Data for offline calibration were acquired from fiber bundles that were mounted in a sample holder and oriented vertically with respect to the probe mounted on an *x–y* stage. At least five Raman spectra were acquired and averaged for each fiber sample used in the calibration. Typical data acquisition parameters were 20 s of acquisition, two accumulations, dark subtraction, and with the cosmic ray filter turned on and the white light correction turned off. The full power of a 400-mW, 785-nm near-infrared laser (Invictus, Kaiser Optical Systems) was injected into a 15-m, 50-μm core multimode excitation fiber. A 15-m, 100-μm multimode collection fiber was used to couple the Raman scatter back into the spectrometer base unit equipped with a 785 nm Holoplex grating. All of the data were recorded with an Olympus LC Plan FI 20x (0.40 NA) ultralong working distance objective. Because the laser radiation was polarized, the probe head was modified to include a quartz wave plate to scramble the input laser polarization. This was done to ensure that the fiber orientation did not affect the measured Raman band intensity and introduce an error in the estimation of crystallinity. In this configuration, the laser typically delivered 100 mW or greater of depolarized laser radiation at the sample. The same optical setup (probe, fiber optics, etc.) used for calibration was also used for the online measurements. The modified Raman probe was mounted on an *xyz* translation stage that was, in turn, mounted on a tripod. We accessed different locations along the spinline by simply raising or lowering the tripod and/or the *z* translation. Because the side to side movement of the fibers in the quench tower significantly reduced the Raman signal, a low friction ceramic guide was used to stabilize the fibers during the Raman measurements. Online Raman spectra were acquired from the fiber bundle under the following conditions: 60 s of acquisition, four accumulations, dark subtraction, and with the cosmic ray filter turned on and the white light correction turned off.

Raman data processing

All spectral acquisition was performed with holograms. The spectra were subsequently transferred to Grams/AI for processing and analysis. Identical data processing was used for the calibration and online data. The raw spectra were smoothed and baseline

TABLE III
Key Properties of the hPP Resins Used for Fiber Spinning

Resin	Description	M_w	M_n	M_w/M_n	MFR (g/10 min)[a]	Density
5D49	Homopolymer	137,400	42,700	3.22	38	0.9
H502-25RG	Homopolymer	173,800	63,600	2.73	25	0.9

M_w = weight-average molecular weight; M_n = number-average molecular weight.
[a] 2.16 kg at 230°C.

corrected. The 650–1800-cm^{-1} spectral region was then normalized to unit area to account for any variation in laser power and/or data acquisition time (due to fiber movement). These preprocessed data were then analyzed with a custom array basic program that measured the peak heights of specified Raman bands and output the results into a MS Excel worksheet.

Fiber spinning

Both hPP resins used in this study (5D49 and H502-25RG) were melt-spun at 225 ± 1°C on a Hills pilot scale with a 1-in. diameter bicomponent extruder with an aspect ratio (length/diameter) of 30:1. Some key properties of these resins are summarized in Table III. Only one side (side A) of the bicomponent extruder was used to spin the fibers, whereas side B was left empty. Constant throughput was maintained with a 2.87-cc/rev Zenith (Sanford, NC) gear pump. The melt pump was operated at 8.3 and 16.6 rpm to yield throughputs of 0.31 and 0.63 ghm, respectively. We measured the actual throughput by setting the desired pump speed and weighing the accrued polymer after 2 min. A round, 60-hole (84.2#8) spinneret was used to extrude the fibers. The spinneret capillary length and diameter were 0.381 and 2.29 mm, respectively. The fibers were quenched with cooling air blown perpendicular to the direction of filament travel. The quench zone was 183 cm long and was located 12.7 cm below the spinneret. The temperature of the quench air, measured with a hot wire anemometer, was 15.4 ± 1°C, and the average flow rate across the quench zone was 0.17 m/s. The fibers were passed around a takeup roll, located 427 cm below the spinneret, and finally taken up on a bobbin with a Barmag SW4 (Charlotte, NC) winder. Fibers from the 5D49 resin were spun at three different spinning speeds (750, 1000, and 1500 m/min) at an extrusion rate of 0.31 ghm, which yielded fiber denier of 3.7, 2.8, and 1.9, respectively. This resin was also spun at an extrusion rate of 0.63 ghm and at three different spinning speeds (750, 1000, and 1500 m/min), which yielded fiber denier of 7.6, 5.7, and 3.8, respectively. H502-25RG was spun at two spinning speeds (750 and 1000 m/min) at a single extrusion rate (0.31 ghm), which yielded fiber denier of 3.7 and 2.8, respectively. Raman crystallinity profiles form these eight measurements were used to validate the fundamental fiber-spinning models.

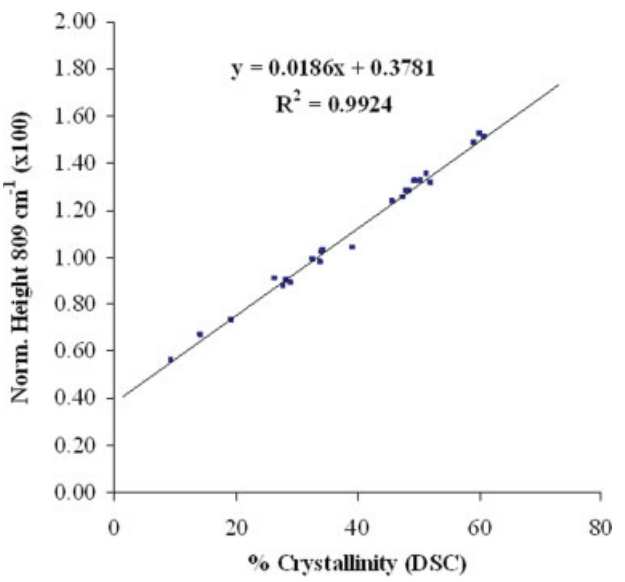

Figure 2 Calibration plot showing the normalized height of the 809-cm^{-1} Raman crystallinity marker regressed against the DSC measured crystallinity. [Color figure can be viewed in the online issue, which is available at www.interscience.wiley.com.]

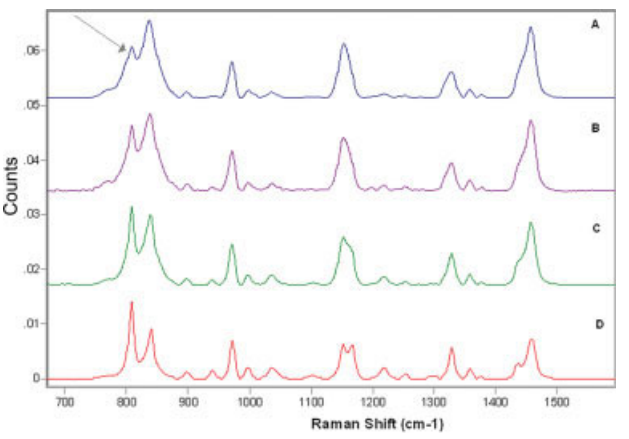

Figure 3 Online Raman spectra for the hPP H502-25RG resin spun at 1000 m/min and 0.31 ghm: (A) 31.1, (B) 33.7, (C) 41.22, and (D) 104.8 cm. [Color figure can be viewed in the online issue, which is available at www.interscience.wiley.com.]

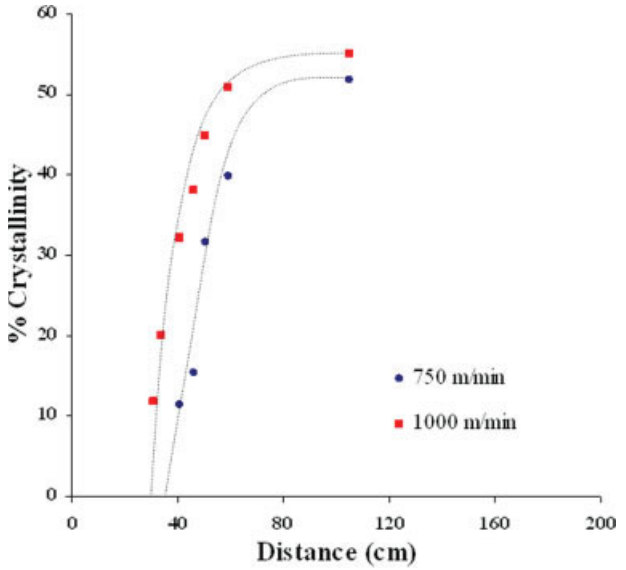

Figure 4 Crystallinity profiles for the 0.31-ghm H502-25 RG fibers at two different spinning speeds. All other spinning conditions were identical. Lines were drawn to guide the eye. [Color figure can be viewed in the online issue, which is available at www.interscience.wiley.com.]

RESULTS AND DISCUSSION

Figure 2 shows the calibration model obtained by the regression of the normalized height of the 809 cm^{-1} Raman crystallinity marker against the DSC-measured crystallinity for the calibration samples. As shown, a good correlation was obtained between the normalized Raman peak height and crystallinity measured via DSC. The calibration curve had a finite intercept. The magnitude of this intercept was similar to the normalized intensity value at 809 cm^{-1} in the Raman spectrum of the melt (data not shown). The presence of two broad Raman bands centered at about 835 and 803 cm^{-1}, observed in the spectrum of the melt (see Fig. 1), resulted in a finite measurable intensity at 809 cm^{-1} even in the amorphous (melt) sample. It is, therefore, not surprising that the calibration curve did not go through the origin. This calibration curve was used to predict the percentage crystallinity from the online Raman spectra measured along the spinline during fiber spinning.

Qualitative evaluation of crystallinity development in the spinline

The online Raman spectra of the H502-25RG fibers obtained as a function of distance from the spinneret are shown in Figure 3. The spectrum obtained 31 cm below the spinneret was consistent with the Raman spectrum of partially molten PP. As the fiber cooled (crystallized), the 809-cm^{-1} band sharpened and also increased in intensity, as evidenced by the Raman spectra shown in Figure 3(B–D). These data were acquired under identical spinning conditions at various distances from the spinneret and illustrated crystallinity development in the spinline for H502-25RG.

Effect of the spinning speed and throughput on the crystallinity

The effect of spinning speed on the measured crystallinity profile is illustrated in Figure 4, with H502-25RG fibers spun at two different takeup speeds (750 and 1000 m/min). The percentage crystallinity values shown are those predicted from the calibration model shown in Figure 2. Representative online Raman spectra of H502-25RG and 5D49 are shown in Figure 5 to qualitatively illustrate the effect of spinning speed on the observed crystallinity. At a fixed point along the spinline, under identical conditions of quench and throughput, the overall crystallinity developed in the fiber increased with increasing spinning speed. This was evidenced by the sharpening and increase in intensity of the 809-cm^{-1} crystalline Raman band with increasing spinning speed. As the spinning speed increased, the point of the onset of crystallization appeared to move closer to the spinneret. Increasing the spinning speed at a constant mass flow rate/throughput increased the stress (molecular orientation) in the fibers, which led to an increase in the rate of crystallization.

Representative crystallinity profiles for 5D49 at two spinning speeds, 750 and 1500 m/min, and two different throughput rates, 0.31 and 0.63 ghm, are shown in Figure 6. At the lower throughput rate, the rise in crystallinity appeared to be more gradual at 750 m/min than at 1500 m/min. The higher spinline stress at 1500 m/min resulted in faster crystallization. At the higher throughput (0.63 ghm), this dif-

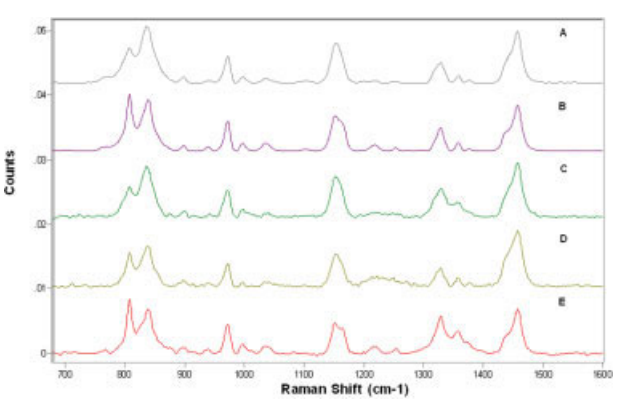

Figure 5 Online Raman spectra of the H502-25RG fibers measured 41 cm below the spinneret at (A) 750 and (B) 1000 m/min and the 5D49 fibers measured 39 cm below the spinneret at (C) 750, (D) 1000, and (E) 1500 m/min. Both resins were spun at a throughput of 0.31 ghm. [Color figure can be viewed in the online issue, which is available at www.interscience.wiley.com.]

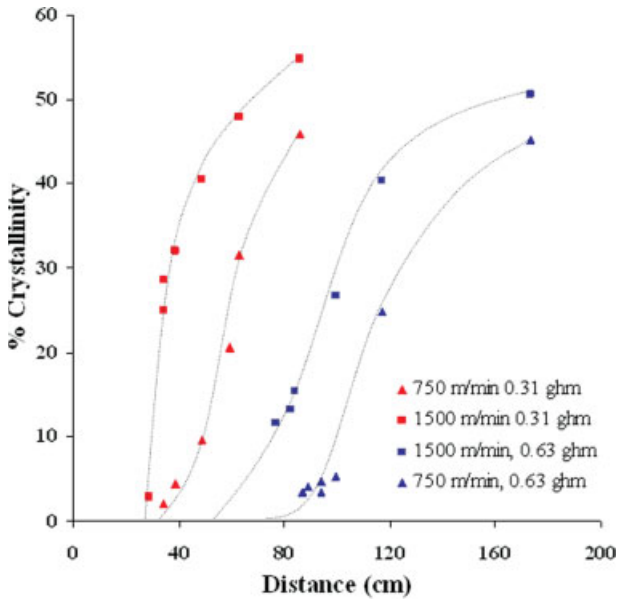

Figure 6 Crystallinity profiles for the 0.31-ghm 5D49 fibers at various spinning speeds. All other spinning conditions were identical. Lines were drawn to guide the eye. [Color figure can be viewed in the online issue, which is available at www.interscience.wiley.com.]

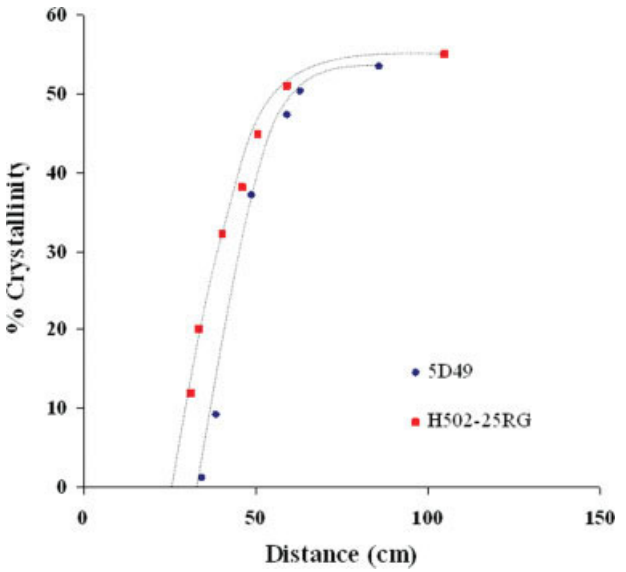

Figure 7 Crystallinity profiles for the 5D49 and H502-25 RG fibers spun at 1000 m/min under identical spinning conditions (0.31 ghm, 0.17 m/s quench). [Color figure can be viewed in the online issue, which is available at www.interscience.wiley.com.]

ference appeared to be less pronounced, although the data acquired at 750 m/min appeared to show more scatter. However, the expected trend was evident when the spinning speed was increased from 1000 to 1500 m/min. At higher throughput, it is likely that spinning speeds in excess of 1500 m/min may be required to build enough stress in the spinline to see a significant difference in the slopes of the crystallinity profiles.

The effect of increasing the throughput at constant spinning speed is also evident from Figure 6. Under identical conditions of quench, increasing the throughput at constant spinning speed would increase the fiber denier. However, the spinline tension decreased only slightly. The net result was a decrease in spinline stress and, consequently, a decrease in the rate of crystallization. Conversely, a lower extrusion rate would result in a higher draw-

TABLE IV
Crystallinity Profile Data for H502-25RG and 5D49 Fibers Spun at Different Conditions

Resin H502-25RG: 0.31 ghm			Resin 5D49: 0.31 gph			
Distance (cm)	750 m/min	1000 m/min	Distance (cm)	750 m/min	1000 m/min	1500 m/min
31	—	11.8%				
34	—	20.0%	34	2.1%	1.1%	26.8%[a]
41	11.5%	32.2%	39	4.4%	9.3%	32.9%
46	15.4%	38.1%	49	9.6%	37.1%	40.5%
51	31.6%	44.7%	59	20.5%	47.2%	—
59	39.8%	50.9%	63	31.6%	50.4%	47.9%
105	51.8%	55.0%	86	45.9%	53.9%	54.8%

Resin 5D49: 0.63 gph

Distance (cm)	750 m/min	Distance (cm)	1000 m/min	Distance (cm)	1500 m/min
87	3.4%	94	4.6%	77	11.6%
94	4.7%	100	7.4%	84	15.5%
100	5.3%	107	16.9%	100	26.6%
117	24.9%	117	28.3%	117	40.4%
173	45.2%	173	43.7%	173	50.7%

Percentage crystallinity was predicted with the calibration model shown in Figure 2. Distances shown are from the spinerette.

[a] Average of two replicate measurements.

down ratio for a given takeup speed; this, in turn, would result in higher spinline stresses. As a result, at a fixed distance from the spinneret, under identical conditions of quench and spinning speed, the fibers spun at higher throughput showed less overall crystallinity, as confirmed from Figure 6.

Effect of the melt index on the crystallinity

It is well known that the molecular weight (MW) and MW distribution of a polymer are important for both the processability of the polymer and the properties of fibers produced from the polymer. Narrower MW distributions improve spinnability. The higher elongational viscosity associated with higher MWs would lead to a more rapid buildup of stress in the spinline with an increase in the takeup speed. This, in turn, would result in a faster and higher buildup of orientation and an increase in the rate of crystallization. Figure 7 compares the effect of melt index on the observed crystallinity for fibers spun at 1000 m/min. As expected, the onset and rate of crystallization of hPP H502-25RG were faster than those of 5D49; similar results were obtained for the H502-25RG and 5D49 fibers spun at 750 m/min.

CONCLUSIONS

Fiber crystallinity data for fibers spun from two hPP resins were obtained on a commercial fiber line with online Raman spectroscopy. These experimental data, presented in Table IV, were used to validate fundamental fiber-spinning models (see part II of this series). The validated models and experimental observations can be used to guide the fiber spinning of hPP for rapid product development. Key results obtained from the online Raman measurements can be summarized as follows: under identical conditions of quench and throughput at a fixed point along the spinline, the overall crystallinity developed in the fiber was found to increase with increasing spinning speed. In addition, as the spinning speed increased, the point of the onset of crystallization moved closer to the spinneret. The rise in crystallinity was more gradual at 750 m/min than at 1500 m/min. Increasing the throughput at constant spinning speed decreased the rate of crystallization because of a decrease in the spinline stress. As a result, at a fixed distance from the spinneret under identical conditions of quench and spinning speed, fibers spun at a higher throughput showed less overall crystallinity. The onset and rate of crystallization were faster in the lower melt index H502-25RG resin than in the 5D49 resin under the spinning conditions explored.

The authors thank Lizhi Liu and Danny King for providing the X-ray crystallinity data, Charles Hagen for running the DSC, and Zeke Rios, Jr., for help with fiber spinning. They also thank Dow Chemical Co. for permission to publish this work.

References

1. Nadella, H.; Henson, H. M.; Spruille, J. E.; White, L. J. J Appl Polym Sci 1977, 21, 3010.
2. Samon, J. M., et al. J Polym Sci Part B: Polym Phys 1999, 37, 1277.
3. Schultz, J. M.; Hsiao, B. S.; Samon, J. M. Polymer 2000, 41, 8887.
4. Ran, S.; Burger, C.; Fang, D.; Zong, X.; Cruz, S.; Hsiao, B.; Chu, B.; Bubeck, R.; Yabuki, K.; Teramoto, Y.; Martin, D.; Johnson, M.; Cunniff, P. Presented at the APS annual meeting, Seattle, WA, March 2001.
5. Seifert, S.; Hsiao, B.; Schultz, J.; Samon, J.; Gurke, I.; Stribec, N.; Saw, C.; Collins, G. Presented at the APS annual meeting, March 1997.
6. Paradkar, R. P.; Sakhalkar, S. S.; He, X.; Ellison, M. S. J Appl Polym Sci 2003, 88, 545.
7. Cherukupalli, S.; Ogale, A. A. Polym Eng Sci 2004, 44, 1484.
8. Paradkar, R. P.; Sakhalkar, S. S.; He, X.; Ellison, M. S. Appl Spectrosc 2001, 55, 534.
9. Analytical Applications of Raman Spectroscopy; Pelletier, M. J., Ed.; Blackwell Science Inc.: Malden, MA; Chapter 4, p 160.
10. Snyder, R. G.; Schachtschneider, J. H. Spectrochim Acta 1964, 20, 853.
11. Neilsen, A. S.; Batchelder, D. N.; Pyrz, R. Polymer 2002, 43, 2671.
12. Hanna, L. A., et al. Polymer 1988, 29, 1843.
13. Tadakoro, H., et al. J Chem Phys 1965, 42, 1432.
14. Massetti, G.; Cabassi, F.; Zerbi, G. Polymer 1980, 21, 143.
15. Kobayashi, M.; Akita, K.; Tadakoro, H. Macromol Chem 1968, 118, 324.
16. Kissin, Y. V.; Rishina, L. A. Eur Polym J 1976, 12, 757.
17. Miyamoto, T.; Inagaki, H. J Polym Sci Part A: Poly Chem 1969, 2, 963.
18. Brooks, A.; Dyke, J.; Hendra, P.; Meehan, S. Spectrochim Acta Part A: Molecular Spectroscopy 1995, 53, 2117.
19. Khafagy, R. J Polym Sci Part B: Polym Phys 2006, 44, 2173.
20. Chalmers, J. M., Edwards, H. G. M.; Lees, J. S.; Long, D. A.; Mackenzie, M. W.; Willis, H. A. J Raman Spectrosc 1991, 22, 613.
21. Ize-Iyamu, M. I. Mater Res Bull 1983, 18, 225.
22. Polypropylene Handbook; Moore, E. P., Jr., Ed.; Hansetr/Gardner: Cincinnati, OH, 1996.
23. Gauer, U.; Wunderlich, B. J Chem Phys Ref Data 1981, 10, 1051.
24. Monasse, B.; Haudin, J. M. Colloid Polym Sci 1985, 263, 822.